Original Article

Access this article online
Quick Response Code:

Website: http://www.braincirculation.org
DOI: 10.4103/bc.bc_76_21

A retrospective anatomical study of the cerebral dural venous sinus outflow pathways utilizing three-dimensional rotational venography

Adrish Anand, Samantha Claire Crowley, Aditya Srivatsan, Visish M Srinivasan, Gouthami Chintalapani[1], Peter Kan[2], Jeremiah N Johnson[3]

Abstract:

OBJECTIVE: Proper blood flow is essential for the maintenance of homeostasis for the human cerebrum. The dural venous sinuses comprise the dominant cerebral venous outflow path. Understanding the spatial configuration of the dural venous sinuses can provide valuable insight into several pathological conditions. Previously, only two-dimensional or cadaveric data have been used to understand cerebral outflow. For the first time, we applied three-dimensional rotational venography (3D-RV) to study and provide detailed quantitative morphological measurements of the terminal cerebral venous sinus system in several pathological states.

SUBJECTS AND METHODS: Patients who underwent a 3D-RV procedure were identified by reviewing our local institution's endovascular database. Patients with high-quality angiographic images were selected. Eighteen patients were included (37.1 ± 3.8 years). Sinuses were divided into four segments, starting at the torcula and ending at the internal jugular vein. Segment length, 3D displacement, and cross-sectional area were measured.

RESULTS: The transverse sinus (60.2 mm) was the longest segment, followed by the sigmoid sinus (55.1 mm). Cross-sectional areas were smallest at the middle of the transverse sinus (21.3 mm^2) but increased at the sigmoid sinus (33.5 mm^2) and at the jugular bulb (49.7 mm^2). The only variation in displacements of venous flow was at the sigmoid-jugular junction, where 55% of cases had lateral displacements versus 45% medial, and 78% superior versus 22% inferior.

CONCLUSIONS: We describe the terminal venous sinus system of patients with a variety of diagnoses, detailing segment length, cross-sectional area, and 3D path.

Keywords:

Cone-beam cerebral venography, dural sinus nomenclature system, three-dimensional rotational angiography, venous sinus outflow

Department of Neurosurgery, Baylor College of Medicine, Houston, Texas, [1]Siemens Medical Solutions USA, Inc., Malvern, Pennsylvania, [2]Department of Neurosurgery, University of Texas Medical Branch, Galveston, Texas, [3]Department of Neurosurgery, University of California at Los Angeles, Los Angeles, California, USA

Address for correspondence:
Dr. Jeremiah N Johnson, UCLA Neurosurgery, 300 Stein Plaza 420, Los Angeles, California 90095, USA.
E-mail: jnjohnson@mednet.ucla.edu

Submission: 20-11-2021
Revised: 29-12-2021
Accepted: 07-01-2022
Published: 21-03-2022

Introduction

The dural venous sinuses comprise the dominant cerebral venous outflow pathways, maintaining intracranial homeostasis.[1] Variations can be associated with idiopathic intracranial hypertension (IIH) and venous sinus stenosis (VSS).[2-4] Despite the importance of these pathways, 3D catheter angiographic studies to describe human venous sinus anatomy are lacking.[5,6] To date, Magnetic resonance venography and Computed tomography venography have been the

How to cite this article: Anand A, Crowley SC, Srivatsan A, Srinivasan VM, Chintalapani G, Kan P, *et al*. A retrospective anatomical study of the cerebral dural venous sinus outflow pathways utilizing three-dimensional rotational venography. Brain Circ 2022;8:38-44.

primary means of evaluation of the cerebral venous system but are prone to artifact.[7] Recently, three-dimensional cone-beam rotational angiography (3D-RA) has been used to evaluate cerebral venous sinuses with additional sensitivity and diagnostic power.[8-10] The use of 3D rotational venography (3D-RV) in clinical diagnostics has allowed for 3D quantitative morphological study of terminal venous dural sinus outflow channels.[11]

Subjects and Methods

Inclusion criteria

We reviewed our institution's endovascular database for patients who underwent advanced 3D-R venography from August 25, 2015 to October 12, 2018. Our local institutional review board approved this retrospective study of patients who underwent 3D-RV, although all imaging was performed for clinical evaluation and not for the purposes of research. Of the 34 cases identified and analyzed, 18 were selected for inclusion in this study based on the condition that images were of sufficient quality and that all necessary measurements could be made from the 3D angiogram reconstruction.

For this study, data were obtained from patients with diagnoses for which venous imaging was felt to be clinically indicated [Supplementary Table 1]. One notable patient subgroup is those with lumbar puncture-proven elevated cerebrospinal fluid (CSF) pressure, papilledema, and bilateral VSS on noninvasive imaging. In these cases, immediately preangiogram, a lumbar puncture was performed, and CSF pressure was reduced to 10–15 mm H20 closing pressure. Angiography and venous pressure manometry were performed if 3D-RV confirmed bilateral VSS. Subsequently, venous sinus stenting was offered to patients who met both angiographic and venous pressure gradient criteria. Patients with documented elevated CSF pressure who were not found to have venous sinus outflow restriction or another underlying cause were considered to have IIH. In this study, patients were split into two groups: patients with vascular issues (VSS or IIH, $N = 10$) or nonvascular (intracranial mass or pulsatile tinnitus, $N = 8$).

Summary of angiographic three-dimensional protocol

The imaging protocol followed the same procedure as described by Srinivasan *et al*.[7] Standard cone-beam 3D-RA imaging was used, with a 5-Fr catheter placed in the internal carotid artery, set to deliver 18 mL of contrast with a 2.5 ml/s injection rate. This imaging technique involves one or two rotational acquisitions, each lasting 4 to 5 s, on flat-panel fluoroscopy equipment after injection of contrast. 3D-RV imaging adjusts for opacification of the venous system via delay of X-ray capture by, on average, 8 to 9 s.[8]

Venous sinus segments

To facilitate analysis of the 3D structure of each segment of the cerebral venous drainage from the confluence of sinuses (torcula) to the end of the internal jugular vein on the 3D reconstruction, the cerebral venous drainage was divided into four segments [Figure 1]. Segment 1 spans from the midpoint of the torcula and terminates immediately before the downward turn where the superior petrosal sinus typically drains into the transverse sigmoid junction. Segment 2 consists of the vertical portion of the sigmoid sinus. To accurately measure vessel displacements in each plane, Segment 2 was further split into segment 2a and Segment 2b. Segment 2a starts at the junction of the transverse and sigmoid junction and consists of the vertical portion of the sigmoid sinus that is lateral to the transverse sigmoid junction. Segment 2b starts at the vertical portion of the sigmoid junction that is medial to the transverse sigmoid junction and ends at the junction of the vertical and horizontal portions of the sigmoid junction. Segment 3 consists of the horizontal portion of the sigmoid sinus as it is deflected medially to laterally by the occipital condyle while simultaneously turning anteriorly and slightly upward before entering the jugular bulb where it terminates. This segment possesses a unique 3D configuration as well as interconnections with deep venous collateral pathways. Segment 3 is located at the transition between the posterior temporal bone and occipital bone where the dural sinus transitions from the intracranial space to enter the jugular foramen. The unique turns and interconnections occur when the sigmoid sinus is coursing medial and slightly anteriorly and is sharply deflected against the occipital condyle before coursing lateral and inferior to pass through the jugular foramen into the extracranial jugular vein. In segment 3 and the proximal jugular bulb, the venous outflow pathway interconnects with other accessory venous outflow pathways, such as the deep cervical veins and the vertebral veins, via the condylar veins.[5,6,12] Segment 4 starts at the jugular bulb and terminates at the end of the internal jugular vein at the lowest extent visible on the 3D reconstruction. These subdivisions allowed the terminal venous sinus drainage pathway to be split into four distinct segments while allowing every important curvature of the system to be measured independently, thus, providing an accurate method to quantify the venous anatomy [Figure 1].

Measurement protocol

All segment lengths were measured using the 3D polyline function on a 3D workstation (syngo, Toolbox, Siemens Healthineers, Germany) by Author 1 and Author 2 with guidance from Author 3 to Author 7. With this function, segment lengths were measured in the middle of the vessel lumen in 3D space. Via the software, we measured length in curved segments by

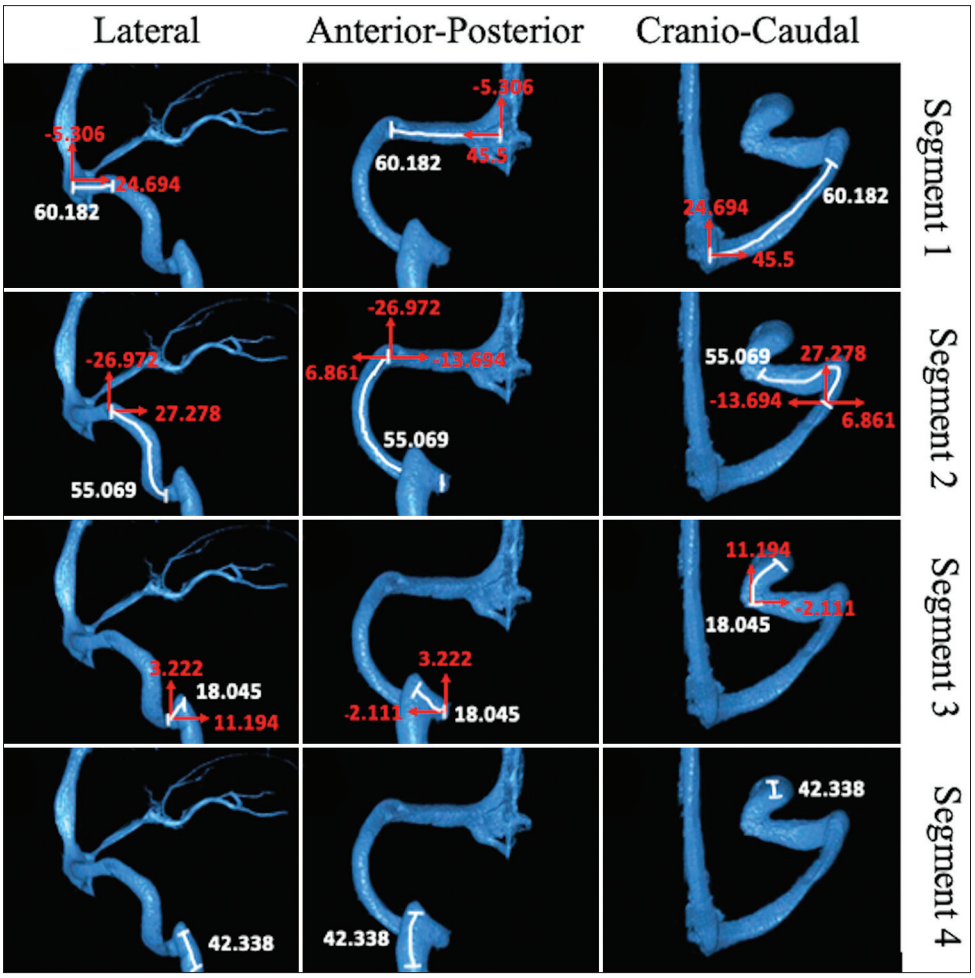

Figure 1: Displacements and lengths of each segment in each axis. Numbers in red and white represent displacement and length of the segment, respectively. The white line demarcates each segment. Anterior, lateral, and superior were assigned positive. Numbers are in millimeters (mm)

establishing multiple points in the middle of the vessel until the end of the segment was reached; thus, any curvature was measured accurately. For each segment, the vessel cross-sectional area was measured at three distinct locations: the start, middle, and the end of the segment. This method may introduce bias regarding differences in vessel caliber at each measured location; however, by measuring at three points we hope to get a good representation of the actual vessel morphology. The end area for one segment was used as the same value for the start area of the subsequent segment. To find the cross-sectional area of a segment, a view perpendicular to the length of the vessel was obtained, while the other two planes were aligned in parallel with the direction of the vessel. The two-dimensional (2D) distance function was used to calculate the major and minor axis of the segment. The area was calculated by using the ellipse area equation (A * B*π), where A and B are half the length of the major and minor axes, respectively [Figure 2]. The ellipse equation was used because past studies on the circularities of the venous sinuses have shown that they are often not circular.[13] By approximating the area as an ellipse, we preserve the curved edges of the cross-section while accounting for the irregularities in the long and short axes.

The displacements of each segment in each plane were measured using the grid function [Figure 3]. The lateral and superior displacements were measured in the posterior-anterior plane; the anterior and superior displacements were measured in the lateral-medial plane; the lateral and anterior displacements were measured in the superior-inferior plane. Each displacement was measured in two complimentary planes and averaged to create one value for each direction. Positive values were assigned to measurements that were lateral, superior, and anterior, while negative values were assigned to measurements that were medial, inferior, and posterior. We did not report blood flow measurements. Reliable quantification of intracranial pressure (ICP) was not presented in this study.

Data analysis

For each patient, 26 data points were collected: length of each segment, the cross-sectional area at the ends

and midpoint of each segment, and the displacement of each segment in 3D space. The mean distances and standard deviations of each of these measurements were calculated. Venous 3D studies were divided into two groups based on the underlying disease being investigated. Group 1 (n = 10) consisted of patients with IIH suspected or confirmed to have underlying VSS. Group 2 (n = 8) consisted of patients who presented with nonhematological problems such as meningiomas or pulsatile tinnitus. To evaluate the differences between these diagnostic groupings, the data points were averaged within each group and a Mann–Whitney U-test was performed (STATA v16.1, College Station, TX, USA). The Mann–Whitney U-test revealed no significant differences for any value between the two groups [Supplementary Table 2]. Corrections for multiple comparisons were not made due to the lack of family-wise statistical comparisons. In addition, we made measurements in patients with several distinct pathological conditions for which venograms were indicated. In some cases, the areas measured may be normal but, in many cases, measurements may be affected by pathology. Consequently, the generalization of our measurements to normal anatomy is limited.

Results

For each data point, average values were calculated for the 18 patients (mean age 38.9 ± 3.7 years). Segment 1 was the longest segment (60.2 ± 3.8 mm) followed by Segment 2 (55.1 ± 3.8 mm). Segment 3 was the shortest segment (18.0 ± 1.7 mm). In general, the transverse sinus traveled laterally (45.5 ± 1.9 mm), inferiorly (5.3 ± 2.0 mm), and anteriorly (24.7 ± 2.3 mm). As it transitioned to the sigmoid sinus, the vessel initially displaced laterally (6.9 ± 1.2 mm) and inferiorly (27.0 ± 2.1 mm) but then curved medially (13.7 ± 2.2 mm) as it continued to descend. Before reaching the jugular bulb, the sigmoid sinus ascends (3.2 ± 1.1 mm), while traveling anteriorly (11.2 ± 0.9 mm). Once the jugular bulb is reached, the vessel travels inferiorly out of the skull, and the cross-sectional area widens from 37.1 ± 3.8 mm^2 in the midpoint of segment 3–49.7 ± 4.6 mm^2 in the extracranial Jugular Vein. For all displacement measurements except for segment 3 lateral and 3 superior, the displacements were in the same direction. For segment 3 lateral, 10/18 (55%) of cases moved laterally from the start of the segment, while 8/18 (45%) moved medially. For segment 3 superior, 14/18 (78%) of cases moved superiorly, while 4/18 (22%) moved inferiorly. The venous cross-sectional area increased along the venous flow path, starting narrow at the transverse sinus (midpoint area 21.3 ± 2.9 mm^2) and gradually increased in segment 2 (midpoint area 35.2 ± 2.6 mm^2) and segment 3 (midpoint area 37.1 ± 3.8 mm^2) until it reached the internal jugular vein (49.7 ± 4.6 mm^2). The displacements and length of each segment can be visualized in Figure 1. The distribution of measurements for all segments can be seen in Figure 4. Exact displacements, segment lengths, and cross-sectional areas can be found in Table 1.

Statistical comparison between venous hypertension and nonvenous hypertension groups yielded no significant results for any of the 26 measurements. Superior displacement for Segment 3 (P = 0.247) was the closest measurement trending toward significance.

Discussion

The results of this study quantitatively describe the lengths and cross-sectional areas of the terminal venous sinus and provide sinus displacement data for the major cerebral venous sinus outflow pathways in the supine position using 3D-RV imaging for several distinct pathological indications. The dimensions and configuration of the venous sinus

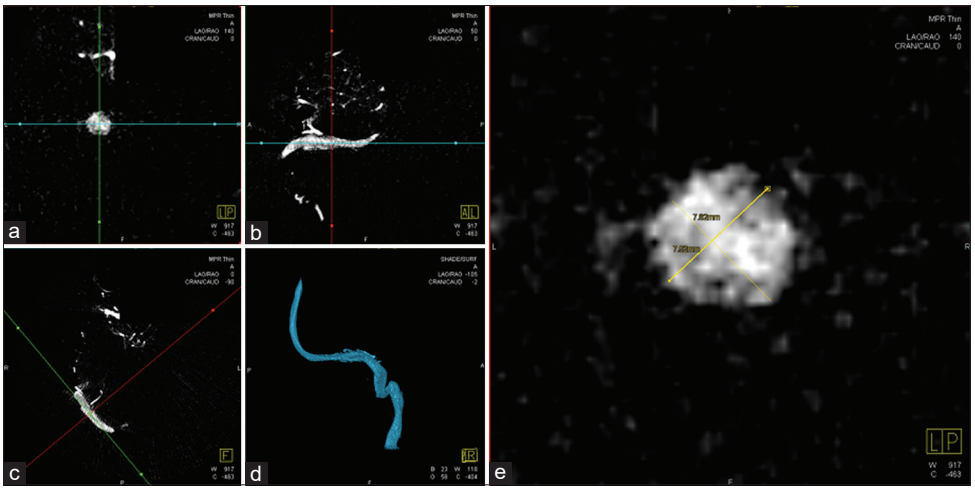

Figure 2: Cross-sectional area measurement at midpoint of transverse sinus. (a-c) Depict venous flow in the coronal, sagittal, and axial plane respectively. (d) is the three-dimensional reconstruction of the venous flow. (e) is a magnified version of A

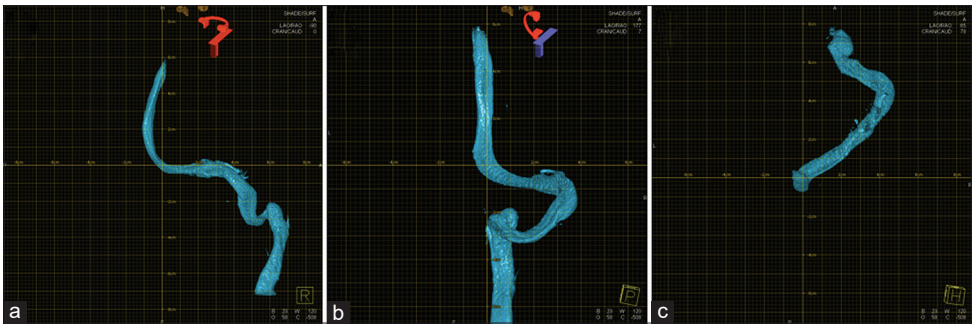

Figure 3: Example of axial displacement measurements for segment 1. (a-c) show the lateral-medial, posterior-anterior, and superior-inferior respectively. To measure segment 1 displacements, the origin is placed at the torcula and the displacement in each direction is measured

Table 1: Average measurements for all data points

Measurement	Length (mm), area (mm^2)
Segment 1	
Length	60.182±3.761
Start area	32.155±4.381
Midpoint area	21.342±2.934
End area	22.578±2.924
Lateral displacement	45.5±1.881
Superior displacement	−5.306±2.08
Anterior displacement	24.694±2.279
Segment 2	
Length	55.069±3.837
Start area	22.578±2.924
Midpoint area	35.169±2.576
End area	33.547±3.503
2a lateral displacement	6.861±1.244
Superior displacement	−26.972±2.118
Anterior displacement	27.278±2.107
2b lateral displacement	−13.694±2.223
Segment 3	
Length	18.045±1.732
Start area	33.547±3.503
Midpoint area	37.128±3.845
End area	49.733±4.587
Lateral displacement	−2.111±2.052
Superior displacement	3.222±1.07
Anterior displacement	11.194±0.889
Segment 4	
Length	42.338±2.499
Start area	49.733±4.587
Midpoint area	51.752±5.097
End area	52.68±6.042

outflow pathways were analyzed with Segment 1 being the longest (60.1 ± 3.7 mm) with the most displacement (45.5 ± 1.8 mm), Segment 3 being the shortest (18.0 ± 1.7 mm) and the narrowest segment being the mid transverse sinus (Segment 1, 21.3 ± 2.9 mm) followed closely by the transverse-sigmoid junction (22.5 ± 2.9 mm). To assess whether the indication for angiography significantly impacted the measurements, patients were categorized into elevated ICP and nonelevated ICP groups: no statistically significant difference for any of the measured parameters was found between the two groups.

In our comparison between the group with elevated ICP vs those without, we may anticipate a difference in the cross-sectional areas of the transverse sinus, indicating some degree of transverse sinus stenosis in the elevated ICP group, but not the other parameters such as length or displacement. Our analysis found that the cross-sectional area nor other measured parameters reached a statistically significant difference between the two groups. One factor to consider when interpreting these findings is in the elevated ICP group, the preangiographic lumbar puncture (as described above) normalized CSF pressures and may have resolved secondary VSS. Thus, the transverse sinus cross-sectional area measurement on 3D-RV studies of IIH/increased ICP patients with transiently normalized pressures were found to have transverse sinus cross-sectional area similar to nonelevated CSF pressure patients. This suggests that much of the transverse sinus and transverse-sigmoid junction stenosis observed in IIH patients may be secondary to compressive effects of CSF on the transverse and sigmoid sinuses or appear exaggerated on noninvasive imaging compared to 3D-RV.

Few studies in the past have studied venous sinus displacement.[14] Our study is the first to quantitatively describe the displacements of the terminal dural venous outflow in all three axial directions. Venous displacement is clinically important because displacements can be altered in pathologies, especially with mass lesions, leading to cerebral edema and IIH.[15,16] In addition, individual differences in sinus displacement might underlie variations in ICP when other structural or physiological causes are absent. One unique finding from this study is the variability in displacements for segment 3. This segment describes the terminal portion of the sigmoid sinus and has unique 3D curvature before joining the jugular bulb and giving rise to multiple extra-jugular outflow venous pathways such as the suboccipital venous plexus and other emissary veins.[5,17]

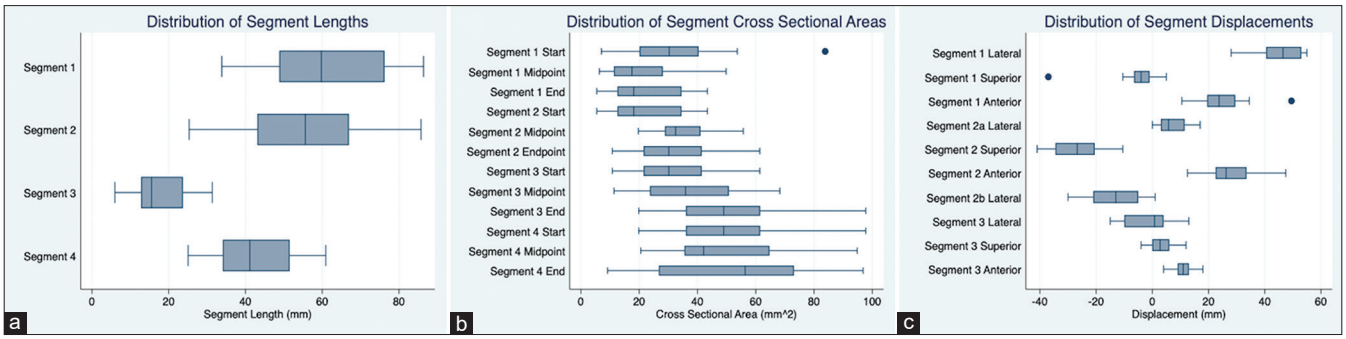

Figure 4: Box plots showing distributions of each measurement. Panel (a) shows distributions for lengths of segments 1–4 in mm. (b) Shows distributions of cross-sectional areas (mm^2). (c) Shows the distribution of displacements for segments 1–3 mm

Cerebral venous imaging is an important screening tool for detecting potential structural venous abnormalities. 3D-RV adds to other 2D venous imaging techniques because it allows for visualization of vessels from multiple views, therefore, improving visualization of vessels which may be superimposed onto each other in 2D and allows for identification and measurement of stenosis sometimes not seen in 2D.[11,18] Additionally, 3D venography provides advantages over other 3D techniques because it allows for better visualization of the deep veins and it allows for fusion with other 3D images to get a better estimate of venous morphology relative to the soft tissue.[7] Few prior studies have utilized 3D venous imaging to visualize and quantify the morphology of cerebral veins in various settings such as in visualization of Sylvian veins and other vessels in brain tumors; however, our study is the first to assess the morphology of the terminal venous dural sinus outflow tracts with high-quality *in-vivo* 3D-RV images.[19,20] Future directions for rotational 3D cerebrovenous imaging may include adaptations to detect dynamic and/or temporary changes to venous outflow pathways dimensions and real-time flow pattern alterations in various physiological states. Limitations of this study include the small sample size and the fact that all subjects had some suspected underlying pathology for which angiography was indicated; hence, the sample may not be representative of an asymptomatic population. Heterogeneity of presenting pathologies may also be a confounding factor in statistical tests. Given the small sample size, any rejection of the null hypothesis should be taken with caution. In addition, because some measurements were taken by user measurement, operator error may introduce minor inaccuracy as compared to using automated software. Furthermore, all measurements were made on a single vendor's processing software, introducing additional possible bias. Finally, the cross-sectional area was approximated using an ellipsoid shape formula, which is not exact but provides the best possible approximation available. Utilizing other imaging modalities or functions to measure vessel morphology will further validate our study results.

This study chose not to evaluate the superior sagittal sinus to focus attention on the terminal venous sinus system, which is prone to stenosis, septations, and webs. It has been proposed that this area has a role in promoting turbulent flow,[2] and there are robust interconnections between the pharyngeal plexus, basilar plexus, and vertebral venous plexus.[21]

Overall, this work utilizes a database of patients who underwent 3D-RV, providing an in-depth description of the terminal dural venous sinus anatomical dimensions and 3D course.

Conclusions

Venous 3D-RV reconstructions provide 3D data regarding the anatomy of the cerebral dural venous sinuses in various clinical states. Using a detailed segmented nomenclature system, venous sinus segment length, cross-sectional area, and 3D path were measured and reported. No difference was detected in the venous outflow pathway parameters measured between IIH patients with temporarily normalized CSF pressures, and those with other indications for venous 3D angiography, possibly indicating resolution of transverse sinus stenosis after ICP correction in some patients. As technology allows a better understanding of cerebral venous outflow, further insight into its role in cerebral homeostasis and its potential role in disease states may be gained.

Financial support and sponsorship

Nil.

Conflicts of interest

Gouthami Chintalapani reports being an employee at Siemens Medical Solutions USA, Inc. No other authors disclose conflicts of interest.

References

1. Kiliç T, Akakin A. Anatomy of cerebral veins and sinuses. Front Neurol Neurosci 2008;23:4-15.

2. McCormick MW, Bartels HG, Rodriguez A, Johnson JE, Janjua RM. Anatomical variations of the transverse-sigmoid sinus junction: Implications for endovascular treatment of idiopathic intracranial hypertension. Anat Rec (Hoboken) 2016;299:1037-42.
3. Morris PP, Lachman N, Black DF, Carter RA, Port J, Campeau N. Increased curvature of the tentorium cerebelli in idiopathic intracranial hypertension. AJNR Am J Neuroradiol 2017;38:1789-93.
4. Buch K, Groller R, Nadgir RN, Fujita A, Qureshi MM, Sakai O. Variability in the cross-sectional area and narrowing of the internal jugular vein in patients without multiple sclerosis. AJR Am J Roentgenol 2016;206:1082-6.
5. Reis CV, Deshmukh V, Zabramski JM, Crusius M, Desmukh P, Spetzler RF, *et al.* Anatomy of the mastoid emissary vein and venous system of the posterior neck region: Neurosurgical implications. Neurosurgery 2007;61:193-200.
6. Doepp F, Schreiber SJ, von Münster T, Rademacher J, Klingebiel R, Valdueza JM. How does the blood leave the brain? A systematic ultrasound analysis of cerebral venous drainage patterns. Neuroradiology 2004;46:565-70.
7. Srinivasan VM, Chintalapani G, Duckworth EA, Kan P. Advanced cone-beam CT venous angiographic imaging. J Neurosurg 2018;129:114-20.
8. Khandelwal N, Agarwal A, Kochhar R, Bapuraj JR, Singh P, Prabhakar S, *et al.* Comparison of CT venography with MR venography in cerebral sinovenous thrombosis. AJR Am J Roentgenol 2006;187:1637-43.
9. Desai H, Yu H, Ohana E, Gunnell ET, Kim J, Isaacson A. Comparative analysis of cone-beam CT angiogram and conventional CT angiogram for prostatic artery identification prior to embolization. J Vasc Interv Radiol 2018;29:229-32.
10. Srinivasan VM, Schafer S, Ghali MG, Arthur A, Duckworth EA. Cone-beam CT angiography (Dyna CT) for intraoperative localization of cerebral arteriovenous malformations. J Neurointerv Surg 2016;8:69-74.
11. Young CC, Morton RP, Ghodke BV, Levitt MR. Retrograde 3D rotational venography (3DRV) for venous sinus stent placement in idiopathic intracranial hypertension. J Neurointerv Surg 2018;10:777-9.
12. Matsushima T, Rhoton AL Jr., de Oliveira E, Peace D. Microsurgical anatomy of the veins of the posterior fossa. J Neurosurg 1983;59:63-105.
13. Lublinsky S, Friedman A, Kesler A, Zur D, Anconina R, Shelef I. Automated cross-sectional measurement method of intracranial dural venous sinuses. AJNR Am J Neuroradiol 2016;37:468-74.
14. Qureshi AI, Qureshi MH, Majidi S, Gilani WI, Siddiq F. Dural venous sinuses distortion and compression with supratentorial mass lesions: A mechanism for refractory intracranial hypertension? J Vasc Interv Neurol 2014;7:35-42.
15. Higgins JN, Burnet NG, Schwindack CF, Waters A. Severe brain edema caused by a meningioma obstructing cerebral venous outflow and treated with venous sinus stenting. Case report. J Neurosurg 2008;108:372-6.
16. Czernicki Z, Grochowski W, Uchman G, Tychmanowicz K, Razumowski AE. Occlusion of the superior sagittal sinus caused by meningioma, intracranial volume-pressure relations and brain edema. Neurol Neurochir Pol 1991;25:580-6.
17. Qureshi AI. A new draining or emissary vein originating from terminal segment of sigmoid venous sinus? J Vasc Interv Neurol 2014;7:39-40.
18. Nishio A, Takami T, Ohata K, Hara M, Mitsuhashi Y, Yokote H, *et al.* Three-dimensional rotation venography using the digital subtraction angiography unit with a flat-panel detector: Usefulness for the transtemporal/transtentorial approaches. Neuroradiology 2004;46:876-82.
19. Kashimoto K, Asai K, Kinoshita M, Okita Y, Tanabe S, Yamane Y, *et al*. A novel protocol for three-dimensional rotational venography with low-dose contrast media in preoperative angiography of brain tumours. Neuroradiol J 2019;32:452-7.
20. Hashimoto Y, Matsushige T, Ogawa T, Sakuragouchi H, Shimonaga K, Takahashi H, *et al.* Impact of cone-beam computed tomography angiography on visualization of sylvian veins. World Neurosurg 2020;143:e206-14.
21. Tubbs RS, Hansasuta A, Loukas M, Louis RG Jr., Shoja MM, Salter EG, *et al.* The basilar venous plexus. Clin Anat 2007;20:755-9.

Supplementary Table 1: Summary of clinical data for all patients undergoing three-dimensional rotational venography

Case number	Reason for angiography	Anesthesia	Noninvasive imaging	Abnormality on noninvasive imaging	Advanced venous imaging	Outcome/intervention
1	Venous sinus stenosis, clinical IIH, jugular vein occluded	GETA	MRA	Lateral left transverse sinus stenosis	3D-RV, Dual volume w/stent, Dyna CTV	Venous stenting
2	Left asterion meningioma	MAC	MR T2 only	Meningioma infiltration of left transverse-sigmoid junction	3D-RV, Dyna CTV	Left transverse sinus focal stenosis
3	Right parasagittal meningioma	MAC	MRV	Meningioma compression of superior sagittal sinus	3D-RV, Bilateral 3D-3D fusion	Angiographic study Demonstrates patent Superior sagittal sinus with trickle flow anterior to the tumor
4	Left parietal parasagittal mass	MAC	MRI	Mass compression of superior sagittal sinus	3D-RV, bilateral 3D-3D fusion	Embolized b/l MMA
5	Pulsatile tinnitus	GETA	CT	Aneurysm at left transverse-sigmoid junction	Dyna CTV, 3D-RV	Balloon assisted coiling
6	Pulsatile tinnitus	GETA	CT	Aneurysm at left transverse-sigmoid junction	Dyna CTV, 3D-RV	Balloon assisted coiling
7	Pulsatile tinnitus	GETA	MRI, MRA	None	3D-RV	Dx only
8	R/O sinus stenosis/ thrombus	MAC	MRV	None	3D-RV	Normal anatomy no intervention
9	Falcine meningioma	CS	MRI	Meningioma occlusion of frontal superior sagittal sinus	3D-RV	Angio, occluded Superior sagittal Sinus from tumor
10	Idiopathic intracranial Hypertension	MAC	MRV	None	3D-RV	VP shunt
11	Falcine meningioma	CS	MRI	Meningioma occlusion of superior sagittal sinus	3D-RV	Dx only
12	Venous sinus stenosis	MAC	MRI, MRV	Bilateral transverse sinus stenosis	3D-RV	Venous stenting
13	Intracranial hypertension	CS	MRI, MRV	None	3D-RV	Dx only
14	Intracranial hypertension	MAC	MRI, MRV	None	3D-RV	Dx only
15	Intracranial hypertension	MAC	CTA, MRI	None	3D-RV	Dx only
16	Intracranial hypertension	General	MRV	None	3D-RV poststenting	Stent placed successfully
17	Intracranial hypertension	MAC	MRV	Slightly narrow right transverse sinus near torcula with no flow obstruction	3D-RV	Dx only
18	Intracranial hypertension	MAC	MRV	Slight stenosis of right lateral transverse sinus near sigmoid junction with no flow obstruction	3D-RV	DX only

GETA: General endotracheal anesthesia, MAC: Monitored anesthesia care, MRA: Magnetic resonance angiography, CS: Combined spinal, MRV: Magnetic resonance venography, CTA: Computed tomography angiogram, CTV: Computed tomography venogram, Dx: Diagnosis, VP: Ventriculoperitoneal, LICA: Left internal carotid artery, MMA: Middle meningeal artery, 3D-RV: Three-dimensional rotational venography, IIH: Idiopathic intracranial hypertension

Supplementary Table 2: Group 1 and Group 2 Comparison

Measurement	*P*
Segment 1	
Length	0.929
Start area	0.79
Midpoint area	0.328
End area	0.79
Lateral displacement	0.859
Superior displacement	0.348
Anterior displacement	0.286
Segment 2	
Length	0.286
Start area	0.79
Midpoint area	0.594
End area	0.595
2a Lateral displacement	0.562
Superior displacement	0.197
Anterior displacement	0.859
2b Lateral displacement	0.307
Segment 3	
Length	0.286
Start area	0.595
Midpoint area	0.79
End area	0.722
Lateral displacement	0.286
Superior displacement	0.247
Anterior displacement	0.859
Segment 4	
Length	0.722
Start area	0.722
Midpoint area	0.424
End area	0.248

A two-sample unequal variance Mann–Whitney *U*-test test was performed for each data point with significance value set at $P<0.05$